journal

J. Am. Ceram. Soc., 94 [6] 1931–1939 (2011)
DOI: 10.1111/j.1551-2916.2010.04318.x

Stabilization Mechanisms of $LaFeO_3$ (010) Surfaces Determined with First Principles Calculations

Chan-Woo Lee,[‡] Rakesh K. Behera,[‡] Satoshi Okamoto,[§] Ram Devanathan,[*,¶] Eric D. Wachsman,[*,‖] Simon R. Phillpot,[*,‡] and Susan B. Sinnott[*,†,‡]

[‡]Department of Materials Science and Engineering, University of Florida, Gainesville, FLorida 32611-6400

[§]Oak Ridge National Laboratory, Materials Science & Technology Division, Oak Ridge, Tennessee 37831-6071

[¶]Pacific Northwest National Laboratory, Chemical and Materials Sciences Division, Richland, Washington 99352

[‖]University of Maryland Energy Research Center, University of Maryland, College Park, Maryland 20742

Density functional theory is used to determine the stabilization mechanisms of $LaFeO_3$ (010) surfaces over a range of surface oxygen stoichiometries. For the stoichiometric LaO surface, and for reduced surface terminations, an electron-rich surface is needed for stabilization. By contrast, in the case of the stoichiometric FeO_2 surface and oxidized surface terminations with low-coordinated oxygen atoms, a hole-rich surface is needed for stabilization. The calculations further predict that low coordinated oxygen atoms are more stable on LaO-type surface terminations than on FeO_2-type surface terminations due to relatively strong electron transfer. In addition to these electronic effects, atomic relaxation is found to be an important contributor to charge compensation, with LaO-type surface terminations exhibiting larger atomic relaxations than FeO_2-type surface terminations. As a result, there is a significant contribution from the sublayers to charge compensation in LaO-type surface terminations.

I. Introduction

ABO_3-TYPE perovskites containing La, Ba, and Sr on the A sites and transition metals, such as Mn, Fe, Co, and Ni, on the B sites are candidate materials for cathodes in solid oxide fuel cells (SOFCs). An important feature of SOFC cathode materials is their ability to reversibly adsorb oxygen on the surface and to incorporate it into the lattice. This adsorption occurs through changes in the oxidation state of multivalent atoms within the material without altering the overall bulk crystal structure.[1,2] $LaFeO_3$-based perovskites (LFOs), especially $La_{1-x}Sr_xCo_yFe_{1-y}O_{3-\delta}$ (LSCF), have been considered for use as cathode materials in so-called intermediate-temperature (IT) SOFCs that operate at temperatures of 500°–700°C, which are low compared with standard devices (700°–1000°C). The IT SOFCs rely, in part, on the high catalytic activity of the cathode for oxygen reduction reactions, and a high ionic and electronic conductivity compared with cathode materials for standard SOFCs, such as $La_{1-x}Sr_xMnO_{3-\delta}$ (LSM). While LFO is itself an insulator, the presence of dopants such as Sr and Co yields a conductive system.

In this work, the structure of the LFO (010) (1×1) surfaces with various terminations are determined, with particular attention paid to the role of electronic redistribution and atomic relaxation on surface stability. The results can be used in the future to quantify the contributions of dopants on performance. Differences in the compensation mechanisms of surface terminations with and without low-coordinated surface oxygen atoms (O_{low}) are also analyzed.

II. Computational Details

(1) Density Functional Theory Calculations

The density functional theory (DFT) calculations are carried out using the Vienna *Ab initio* simulation Package.[3,4] Projector-augmented wave potentials are used with valence configurations of $5s^25p^65d^16s^2$, $3p^63d^64s^2$, and $2s^22p^4$ for La, Fe, and O atoms, respectively. The spin-polarized generalized gradient approximation (GGA) functional parameterized by Perdew, Burke, and Ernzerhof is used to describe exchange and correlation energies of electrons.[5] The magnetic moments of Fe atoms are treated collinearly.

Based on convergence tests of the total energy and lattice constant of bulk LFO, plane waves with an energy cutoff of 600 eV are used for expanding the electronic wave functions. $3 \times 3 \times 3$ and $3 \times 3 \times 1$ k-points Monkhorst–Pack[6] meshes are used for integrations over the Brillouin zone of bulk LFO and the (010) surface, respectively. The ionic relaxation is performed until the Hellmann–Feynman force on each atom is less than 0.01 eV/Å. The density of states (DOS) is broadened by Gaussian smearing with a width of 0.1 eV. As is typical in purely DFT calculations; the results reported here are for zero Kelvin and perfect vacuum.

DFT calculations with the Hubbard correction for Coulomb repulsion (DFT+U method)[7] are often used in calculating the electronic structures of many bulk oxides.[8,9] However, the validity of DFT+U for predicting the stabilities of oxide surfaces is still not well established,[10] and therefore this approach is not used here.

(2) $LaFeO_3$ Surface Structure

Because of the effect of surface composition on oxygen reduction reactions,[11] it is necessary to characterize the stabilities of various cathode surfaces, including nonideal, off-stoichiometric surface terminations that may be stabilized by the operating conditions of the SOFCs. In particular, it is possible that surface terminations with O_{low} atoms may be preferentially stabilized at intermediate operating temperatures. Indeed, it has been reported for several metal oxides that ideal stoichiometric surface terminations are favorable only at low P_{O_2} and/or high temperatures.[12–14]

I. Tanaka—contributing editor

Manuscript No. 27655. Received March 12 2010; approved November 8 2010.

This work was supported by DOE through the High Temperature Electrochemistry Center (HiTEC) at University of Florida, Contract No. DE-AC05-76RL01830.
Work by S. O. is supported by the Division of Materials Sciences and Engineering, Office of Basic Energy Sciences, U.S. Department of Energy.

*Member, The American Ceramic Society.

†Author to whom correspondence should be addressed. e-mail: ssinn@mse.ufl.edu

Electronic structure calculations are powerful tools to investigate the stabilities of different surface stoichiometries because the geometry of the system can be fully controlled at the atomic level. Using a combination of DFT and thermodynamics, Kotomin *et al.*[15] showed that the MnO_2-terminated cubic $LaMnO_3$ (001) surface with adsorbed O atoms is energetically stable under typical SOFC-operating temperatures and P_{O_2}. Recently, Mastrikov *et al.*[16] predicted that the O_2-terminated (011) surface and MnO_2-terminated (001) surface of cubic $LaMnO_3$ are the most stable of eight different surface terminations of (001), (110), and (111) planes.[15]

Liu *et al.*[17] reported from DFT calculations that surface Fe on the FeO_2-terminated surface of LFO (010) is the most favorable site for O_2 adsorption. Additionally, Lee *et al.*[18] calculated the energetics of oxygen–perovskite interactions, such as adsorption energy and formation energy of surface oxygen vacancies. They also explored the effects of the Hubbard correction and magnetic state of the oxide to these energetics.[18] However, to the best of our knowledge, no studies have yet analyzed the combination of electronic structure, stochiometry, and surface atomic relaxation associated with the LaO- and FeO_2-type terminations of LFO, as is carried out here.

LFO has the *Pnma* structure ($P\,2_1/n\,2_1/m\,2_1/a$, space group #62) as indicated in Fig. 1(a). The *Pnma* structure is derived from the ideal cubic perovskite with $Pm\bar{3}m$ structure (#221). In the *Pnma* structure, the oxygen octahedra are tilted with respect to their neighbors in a repeating pattern.[19] This octahedral tilting both breaks the symmetry of the $Pm\bar{3}m$ $\langle 001\rangle$ directions and increases the size of the unit cell from one formula unit (5 atoms) to four formula units (20 atoms). The [100] and [001] directions of the *Pnma* unit cell are aligned with the $[10\bar{1}]$ and [101] directions in the $Pm\bar{3}m$ cubic perovskite structure. The [010] directions in the two structures are the same, as illustrated in see Fig. 1(b). Thus, in the *Pnma* space group the three surfaces with alternating AO and BO_2 layers are $(10\bar{1})$, (101), and (010). For the studies described here we choose the (010) surface. In the (010) surface, each atomic layer contains two LaO or two FeO_2 units, as indicated in Fig. 1(b).

Although their dimensions are slightly different due to the octahedral tilting, the $(10\bar{1})$ and (101) surfaces can be expected to be similar. The corresponding surfaces in various other perovskites, including $BaTiO_3$, $SrTiO_3$, and $LaAlO_3$, have been extensively examined experimentally and theoretically.[20–26]

The surface slab models are built with a (1×1) surface unit cell within the plane of the surface. To determine the energy dependence on surface unit cell size, we compare the total energies of the LaO surface termination with (1×1) and (2×2) surface unit cells, where each slab has a thickness of 11 atomic layers. The resulting surface energy difference between the two systems is 0.1 meV/Å^2. Considering that surface energy is on the order of 1.0 eV/Å^2, and the differences in the surface energies of the structures considered are >0.2 meV/Å^2, this difference is sufficiently small to justify the use of the (1×1) surface unit cell in the work shown here. The surface energy, ω is defined in the usual manner as

$$\omega = \frac{1}{2A}\left(G^{\text{slab}} - \sum_i \mu_i N_i\right) \quad (1)$$

where G^{slab} is the Gibbs-free energy of the surface slab, which is equivalent to the total energy from the DFT calculations in these zero Kelvin and zero pressure calculations in the absence of vibrational contributions. In q. (1), A is the surface area; the index i runs over all atomic species in the system (in this case, La, Fe, and O), μ_i is the chemical potential of the i-th component in the bulk unit from which the surface is constructed, and N_i is the number of each atomic species. The factor of 1/2 arises because the symmetric slab contains two equivalent surfaces. The chemical potential of oxygen is determined in the same way as in He and colleagues.[27,28]

Each surface termination considered is built as a symmetric surface slab with a thickness of more than nine atomic layers. The positions of all of the atoms in the system are fully relaxed with the exception of the atoms in the center layer of each slab, which are held fixed.

We constructed the 16 different (010) surface terminations summarized in Table I: seven surface terminations based on the stoichiometric LaO surface termination and nine based on the stoichiometric FeO_2 surface termination. The nomenclature used to describe the various surfaces is based on the number of O atoms that are added to or removed from the topmost LaO and FeO_2 layers. In particular, terminations are denoted LaO+xO, and FeO_2+xO where x describes the number of added or removed O atoms at the surface per one LaO/FeO_2 molecular unit. As there are two FeO_2 or LaO units in each layer of the (1×1) surface unit cell, if there is one O_{low} on the FeO_2 layer, for example, the corresponding surface termination is designated as $FeO_2+0.5O_{low}$. The initial positions for added and removed O atoms are determined from the Wyckoff positions of the corresponding O atoms in bulk LFO. Figs. 2(a)–(c) illustrate the LaO, $LaO+0.5O_{low}$, and $LaO+1.5O_{low}$ surface terminations. Figs. 2(d)–(f) show the FeO_2, $FeO_2+0.5O_{low}$, and $FeO_2+1.5O_{low}$ surface terminations. Hereafter, surfaces with LaO$\pm x$O/O_{low} and $FeO_2\pm x$O/O_{low} surface terminations will be simply designated as LaO-type and FeO_2-type surface terminations, respectively. In all cases, the topmost FeO_2 or LaO layer in contact with the vacuum region is designated as the first layer. For surface terminations with an overlayer of O_{low} atoms, the O_{low} atoms are designated as being in layer zero.

(3) Charge Compensation

It is instructive to construct line diagrams in which the top layers of stoichiometrically different surface terminations are aligned by their layer charges, as is shown in Fig. 3. First, we consider a simple line diagram for the top layer charge, σ°_{1st} (Fig. 3(a)), where the superscript indicates layer charge before charge compensation. All layer charges in Fig. 3 are calculated based on

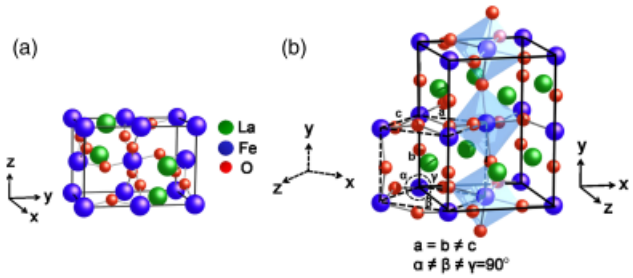

Fig. 1. (a) Schematic of $LaFeO_3$ unit cell. (b) Relative direction of orthorhombic unit cell (solid line) of $LaFeO_3$ to pseudo-cubic cell (dotted line). The oxygen octahedra are shaded light blue.

Table I. Possible Surface Terminations of LFO (010) plane

Type of surface terminations	
LaO-type	FeO_2-type
	FeO_2–2.0O
	FeO_2–1.5O
LaO–1.0O	FeO_2–1.0O
LaO–0.5O	FeO_2–0.5O
LaO	FeO_2
$LaO+0.5O_{low}$	$FeO_2+0.5O_{low}$
$LaO+1.0O_{low}$	$FeO_2+1.0O_{low}$
$LaO+1.5O_{low}$	$FeO_2+1.5O_{low}$
$LaO+2.0O_{low}$	$FeO_2+2.0O_{low}$

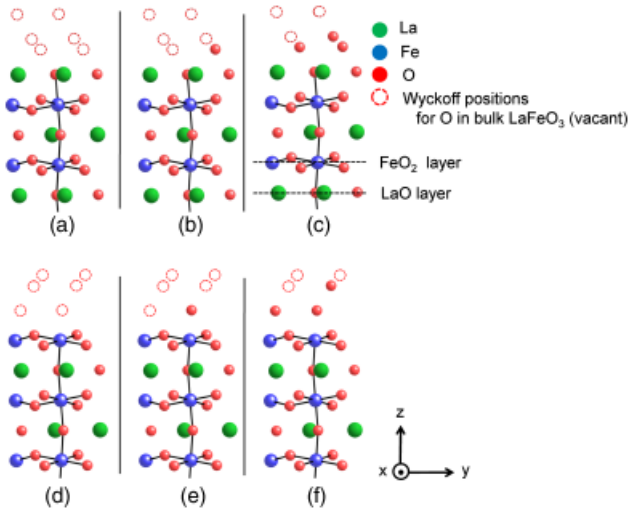

Fig. 2. Schematics of LaO-type surface terminations (a) LaO, (b) LaO+0.5O_{low}, and (c) LaO+1.5O_{low}; and FeO_2-type surface terminations: (d) FeO_2, (e) FeO_2+0.5O_{low}, and (f) FeO_2+1.5O_{low}. Dotted circles are possible Wyckoff positions for O atoms based on the bulk LFO symmetry.

ideal ionic charges of La, Fe, and O in the bulk LFO (La:+3e, Fe:+3e, and O: −2e).

Surface terminations are categorized as terminations with positive or negative σ°_{1st}. All reduced surface terminations have positive or zero σ°_{1st} and all oxidized surface terminations have negative or zero σ°_{1st}. Stoichiometric LaO and FeO_2 surface terminations have σ°_{1st} of $+1.0e$ and $-1.0e$, respectively.

The LFO (010) surface is categorized as a type-III polar surface[29] because the LaO and FeO_2 layers have nonzero ionic charges ($\sigma \neq 0$) and each repeat unit (LaO–FeO_2 bilayers) bears a nonzero dipole moment ($\mu \neq 0$); type-I surfaces have zero layer charge ($\sigma = 0$) and zero dipole moment ($\mu = 0$) and type-II surfaces have nonzero layer charge ($\sigma \neq 0$) and zero dipole moment ($\mu = 0$). Type-III polar surfaces with ideal layer charges are unstable because the electrostatic potential, V, between the surfaces monotonically increases with surface thickness due to the nonzero electrostatic field per repeat unit. The corresponding electrostatic energy is significant and is the source of surface instability.

The contribution of the electrostatic potential to surface instability can be understood by considering a macroscopic surface model, which is illustrated in Fig. 4.[30,31] In particular, we consider polar surfaces consisting of repeat units of bilayers with $+\sigma_B$ and $-\sigma_B$ as their layer charge per unit area, respectively, as is shown in Fig. 4(a). The assumptions for the macroscopic surface model are that the discrete atomic structure inside each layer parallel to the surface can be neglected (e.g., no surface rumpling is considered), and that the electron density in the layers is localized with no charge overlap between the layers. Using this model, the averaged electrostatic field per repeat unit, $\langle E \rangle$, is $\frac{\sigma_B}{2\varepsilon_0}$ and is nonzero. As a result, V increases by $\delta V = \frac{\sigma_B R}{\varepsilon_0}$ per repeat unit of thickness R and increases monotonically with increasing surface thickness, which leads to system instability. Charge compensation of the layer charge cause $\langle E \rangle$ to be equal to $\frac{2\sigma_{1st}-\sigma_B}{2\varepsilon_0}$, which goes to zero when

$$\sigma_{1st} = \frac{\sigma_B}{2} \tag{2}$$

where σ_B is the layer charge of bulk system, and σ_{1st} is the compensated charge of the first layer. Under these conditions, which are illustrated in Fig. 4(b), there is no monotonic increase in potential across the slab. The electronic redistribution in the top surface layer is the largest, but charge compensation in lower layers can still occur, leading to the more general form:[30,31]

$$\left|\sum_{i=1}^{m} \sigma_i\right| = \frac{|\sigma_B|}{2} \tag{3}$$

where σ_i is the layer charge associated with the ith layer, and m is the number of outer layers for which the layer charges are modified.[30,31]

This analysis makes clear that $\Delta\sigma^{\circ}_{1st} = (\sigma^{\circ}_{1st} - \frac{\sigma_B}{2})$ is more useful than σ°_{1st} for understanding surface charge compensation, as Fig. 3(b) also indicates. If $\Delta\sigma^{\circ}_{1st}$ is positive, then additional electrons with magnitude of $|\Delta\sigma^{\circ}_{1st}|$ are needed to achieve charge compensation. On the other hand, if $|\Delta\sigma^{\circ}_{1st}|$ is negative, additional holes that are equivalent in charge to $|\Delta\sigma^{\circ}_{1st}|$ are needed.

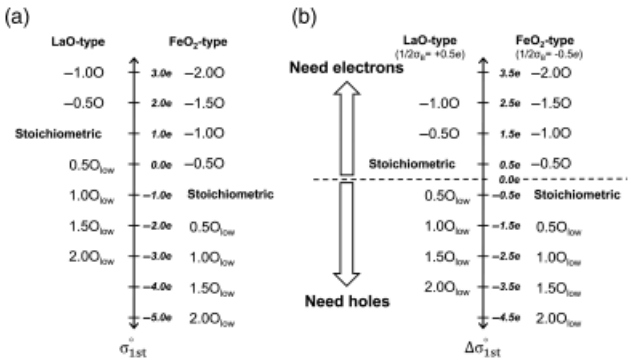

Fig. 3. (a) Line diagram for charges (σ°_{1st}) in the surface layers; (b) Line diagram of $\Delta\sigma^{\circ}_{1st} = (\sigma^{\circ}_{1st} - \frac{\sigma_B}{2})$ of top layers. For (b), "need electrons (holes)" means additional electrons (holes) are required to compensate top layer charge to $\Delta\sigma^{\circ}_{1st} = 0$. Here, all layer charges are calculated based on ideal ionic charges of La, Fe, and O in the bulk LFO.

III. Results and Discussion

(1) Bulk LFO

The calculated lattice constants agree well with experimental values and a previous DFT study.[17,32] In comparison with experimental lattice constants, the largest deviation is an overestimate by 1.725% for the lattice parameter in the a direction. Such overestimates are typical for calculations based on the GGA functional.[33]

Figure 5 illustrates the DOS of bulk LFO. The radii for Wigner–Seitz cells for all DOS results in this paper are determined based on Shannon ionic radii: $r_{La} = 1.16$ Å, $r_{Fe} = 0.65$ Å (high-spin configuration), and $r_O = 1.4$ Å;[34] from Fig. 5, it can be seen that the Fe ions have electrons in high-spin configurations. The calculated Kohn–Sham gap is 1.0 eV, which is less than the experimental band gap of 2.1 eV.[35] Nonetheless, the DFT calculations correctly predict LFO to be insulating, which is consistent with the findings of previous DFT studies.[36,37]

To establish that DFT can correctly determine the structural and magnetic ground states of the system, we compare the total energies of bulk LFO with the $P6_3cm$, $Pm\bar{3}m$, $R\bar{3}c$, and $Pnma$ space groups, with various magnetic states including ferromagnetic, A-type antiferromagnetic (A-AF), C-type antiferromagnetic (C-AF), and G-type antiferromagnetic (G-AF) (see Fig. 6). For $P6_3cm$, A-AF, G-AF, and ferromagnetic states are considered based on the magnetic orderings of $YMnO_3$, which has the same space group.[38] DFT predicts the structural and magnetic ground state of bulk LFO to be $Pnma$ with G-AF, which is consistent with reported experimental results.[37,39,40]

Experimentally, it has been reported that LFO only experiences structural transitions from orthorhombic to rhombohedral ($Pnma \rightarrow R\bar{3}c$) at 1278 ± 5 K,[41] which corresponds to the maximum operating temperature of standard SOFCs. The cubic $Pm\bar{3}m$ symmetry is not available for pristine LFO. This phase transition trend can be understood by the structural order illustrated in Fig. 6, which shows that the energy differ-

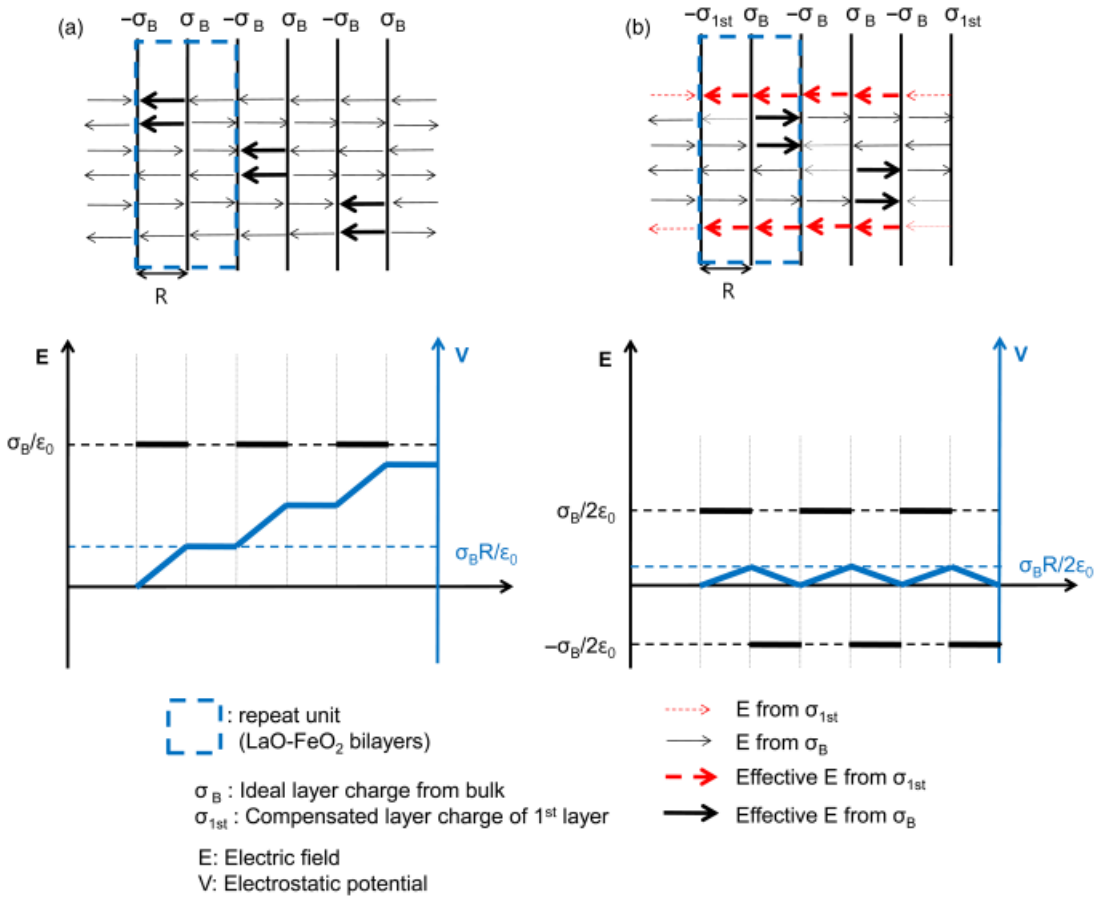

Fig. 4 Spatial variations of the electric field, E, and of the electrostatic potential, V, in a macroscopic surface models cut along a polar direction. (a) When all layers bear σ_B without charge compensation, the electrostatic potential increases monotonically through the sample. (b) The layer charge of top layers is modified by $\sigma_{1st} = \frac{\sigma_B}{2}$: the electrostatic potential no longer shows a monotonic increase through the surface model.[30,31]

ence between ferromagnetic $Pm\bar{3}m$ and G-AF *Pnma* is 0.33 eV/LFO. This is much larger than the energy difference between *Pnma* and $R\bar{3}c$ with G-AF, which is 0.06 eV/LFO.

However, the magnetic state of LFO can be changed from the G-AF to the ferromagnetic state within the range of SOFC operating temperatures due to its Néel temperature of ~740 K.[42] Nonetheless, G-AF is chosen as the magnetic state of the bulk and surfaces of the LFO in this work. This is supported by the fact that the energetics of the cubic ($Pm\bar{3}m$) LFO surface for the G-AF and ferromagnetic state have been reported to be similar with the GGA functional.[18] In particular, it has been reported that the formation energy of an oxygen vacancy on the FeO_2 surface with the G-AF state is higher than that within the ferromagnetic state by ~0.32 eV. This indicates that the surface electronic redistribution caused by the generation of the vacancy would be similar at a FeO_2 surface for both G-AF and ferromagnetic states. However, it must be pointed out that further investigation will be required to fully determine the effect of magnetic and structural ground states on the surface electronic redistribution of the LFO surface.

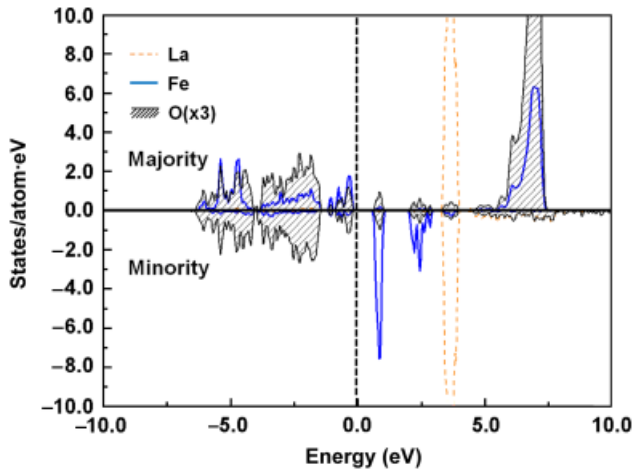

Fig. 5. Electronic DOS of bulk $LaFeO_3$. Electrons in Fe atom have high-spin configuration in which electrons are aligned in the upward direction (majority). E_F is set to zero (vertical dotted line).

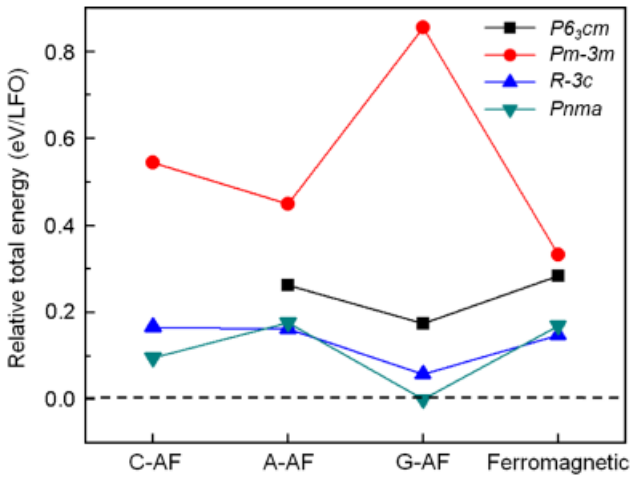

Fig. 6. Total energy comparison of bulk LFO with different space groups relative to space group *Pnma* and magnetic ground state G-AF, which is chosen to be the zero.

(3) Stabilization Mechanisms of the LFO (010) Surface

Three factors will be examined to investigate how the LFO (010) surface is stabilized: (i) the contribution of each atomic species to charge compensation; (ii) the contribution of sublayers; and (iii) the contribution of atomic relaxation.

(A) Contribution of Atomic Species to Charge Compensation: Bader topological analysis[43] is performed on the calculated charge densities of bulk LFO and all surface terminations. The calculated Bader charges of La, Fe, and O atoms in bulk LFO are found to be $q_{\mathrm{La}}^{\mathrm{bulkLFO}} = 2.09e$, $q_{\mathrm{Fe}}^{\mathrm{bulkLFO}} = 1.66e$, and $q_{\mathrm{O}}^{\mathrm{bulkLFO}} = -1.25e$, respectively. The layer charges (σ) are calculated as the sum of Bader charges of atoms in the layer. For example, σ of first layer of $\mathrm{LaO}+0.5\mathrm{O_{low}}$ surface termination is $\sigma_{1\mathrm{st}} = q_{\mathrm{La,1st}} + q_{\mathrm{O,1st}} + 0.5q_{\mathrm{O,low}}$. As seen from Table II, all surface terminations satisfy the condition for surface charge compensation given in Eq. (3) with a maximum deviation of about 8%.

To investigate the contribution of each atomic species (La, Fe, and O) to charge compensation, Bader charges of each atomic species are analyzed in terms of $\langle\Delta q\rangle = \langle q - q^{\mathrm{bulkLFO}}\rangle$, where q and q^{bulkLFO} are Bader atomic charge at the surface and the corresponding Bader atomic charge from bulk LFO $\langle\ldots\rangle$ denotes the average over the surface layer. Atoms with negative $\langle\Delta q\rangle$ have additional electrons relative to their bulk counterparts, while atoms with positive $\langle\Delta q\rangle$ have fewer electrons. Figures 7 and 8 illustrate $\langle\Delta q\rangle$ for the cations in the first and second layers, and for the anions in the zeroth and first layers of the relaxed LaO-type and FeO_2-type surface terminations, respectively.

For reduced surface terminations and stoichiometric LaO surface terminations where electrons are needed for charge compensation (see Fig. 3(b)), the contribution of La and Fe cations is dominant. As indicated in Fig. 7, the La and Fe cations in the relaxed stoichiometric LaO-terminated surface are slightly negative relative to cations in the bulk. This is because there are fewer oxygen anions to accept electrons. In particular, the coordination number of the La in the first layer of the stoichiometric surface is 5, while the coordination of bulk La is 8; the corresponding surface and bulk values for Fe are both 6. When the surface is reduced, there are even fewer oxygen anions available, and so the charge on the surface cations becomes even more negative relative to the bulk, i.e., the surface La and Fe ions are less ionized than in the bulk. This is illustrated by a reduction in coordination to 3 for La and 5 for Fe for the most reduced surface. The surface La and Fe ions achieve a minimum value of about $-0.6e$. In other words, the reduced and stoichiometric LaO-type surfaces achieve neutrality by countering positive $\Delta\sigma_{1\mathrm{st}}^{\circ}$ with a redistribution of charge such that the surface is electron rich.

Table II. Comparison Between the Sum of Surface Layer Charges $\left(\left|\sum_{i=1\,\mathrm{or}\,0}^{m-1}\sigma_i\right|\right)$ and Half of Layer Charge of Bulk LFO $\left(\frac{|\sigma_B|}{2}\right)$

x	m	$\left\|\sum_{i=1\mathrm{or}0}^{m-1}\sigma_i\right\|$	Deviation (%)
LaO-type surface terminations			
−1.0	6	0.413	−1.37
−0.5	6	0.420	0.19
0.0	5	0.439	5.20
0.5	6	0.422	0.66
1.0	4	0.428	2.20
1.5	6	0.428	2.24
2.0	5	0.413	−1.17
FeO_2-type surface terminations			
−2.0	6	0.450	7.65
−1.5	6	0.443	6.12
−1.0	5	0.411	−1.77
−0.5	6	0.431	3.29
0.0	5	0.421	0.56
0.5	6	0.418	0.00
1.0	5	0.429	2.34
1.5	6	0.420	0.57
2.0	6	0.420	0.62

x indicates the stoichiometry of the surface, and $m-1$ is the number of layers over which the sum is carried out. All charges are determined by Bader analysis. For $x>0.0$, the layer number is counted from zero as layers consisting of $\mathrm{O_{low}}$ atoms are designated as zeroth layers. For $x>0.0$, $m=a$ means there are $a+1$ surface layers before center bulk layer. For $x\leq 0.0$, $m=a$ means there are a number of surface layers.

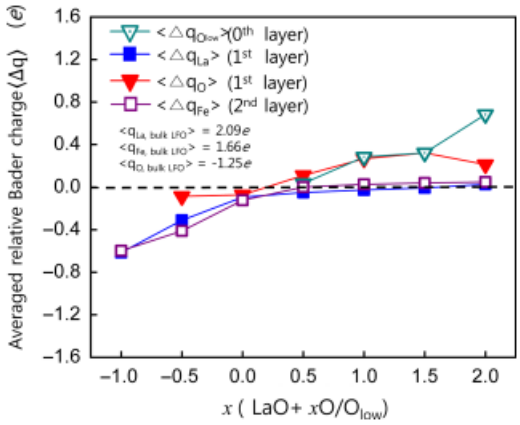

Fig. 7. Averaged relative Bader charge ($\langle\Delta q\rangle = \langle q - q^{\mathrm{bulkLFO}}\rangle$) of surface atoms for relaxed $\mathrm{LaO}+x\mathrm{O/O_{low}}$ surface terminations.

For relaxed oxidized LaO-surface terminations, there is an excess of oxygen ions at the surface and their relative Bader charges are more positive than those of oxygen anions in the bulk, as indicated in Fig. 7. This is because the oxygen ions are undercoordinated to cations and thus have accepted fewer electrons than their bulk counterparts. In the case of the zeroth layer $\mathrm{O_{low}}$ ions, they are slightly more undercoordinated than the first layer oxygen ions (their coordination numbers are 2 and 3, respectively). Therefore, their relative Bader charges are the same as, or more positive than, the oxygen ions in the first layer. Stated another way, the oxidized LaO-type surfaces achieve neutrality by countering negative $\Delta\sigma_{1\mathrm{st}}^{\circ}$ with a redistribution of charge such that the surface is hole-rich.

These effects are similar to the proposed charge compensation mechanism for the $(\sqrt{5}\times\sqrt{5})R26.6^{\circ}$ surface reconstruction (RT5) of the $LaAlO_3$ (001) surface, which contains La vacancies in the La_5O_5 ($V_{\mathrm{La}}La_4O_5$) surface unit cell.[25] The charge distribution at the $V_{\mathrm{La}}La_4O_5$ surface is found to be dominated by oxygen ions that are less negatively charged than bulk oxygen ions. The atomic ratio of the La and O atoms in the top layer, $V_{\mathrm{La}}La_4O_5$ is analogous to the $\mathrm{LaO}+0.25\mathrm{O_{low}}$ surface termination under consideration here.

In the case of the fully stoichiometric FeO_2 surface termination, the relative charges on the Fe and La ions are approxi-

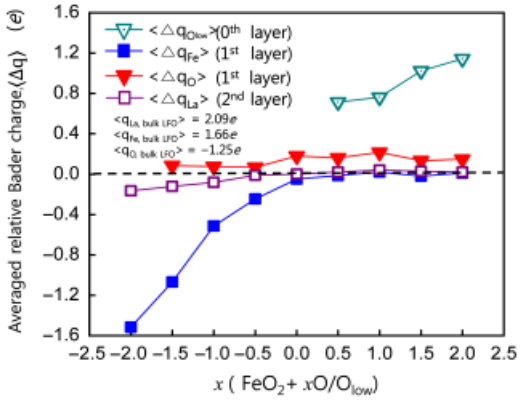

Fig. 8. Averaged relative Bader charge ($\langle\Delta q\rangle = \langle q - q^{\mathrm{bulkLFO}}\rangle$) of surface atoms for relaxed $\mathrm{FeO_2}+x\mathrm{O/O_{low}}$ surface terminations.

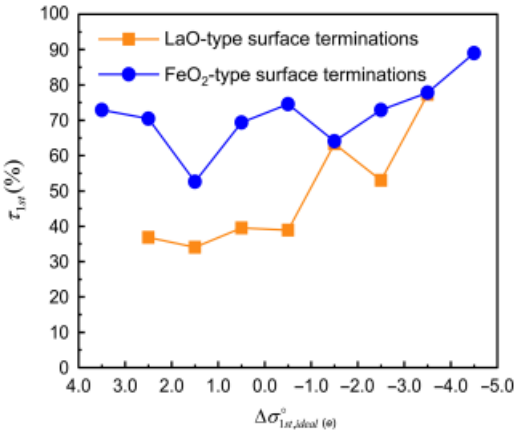

Fig. 9. Percentage of change in charges in the first layer before and after electronic redistribution and layer charge based on bulk LFO. All charges are determined by Bader analysis except $\Delta\sigma^{\circ}_{1st,ideal}$, which is calculated based on ideal ionic charges of La, Fe, and O in the bulk LFO. If τ_{1st} is 100%, charge compensation is achieved only by the first layer.

mately zero relative to the bulk, as indicated in Fig. 8; the surface as a whole is slightly positive relative to the bulk. When the surface is reduced, however, there is a substantial difference in the responses of the Fe and La surface cations. The La cations are slightly negative as they are unable to donate all of their electrons to oxygen ions; they achieve a minimum relative charge of about $-0.2e$. However, the relative charges on the surface Fe cations decrease precipitously to achieve an average value of about $-1.6e$ when the surface is fully reduced. This difference is due to the multivalent nature of the Fe, which exists as Fe^{+3} in LFO but can convert to Fe^{+2} under these types of reducing conditions. As a result, the Fe cations at the reduced surfaces donate even fewer electrons to oxygen ions than bulk Fe. In other words, the reduced surfaces again achieve neutrality by countering positive $\Delta\sigma^{\circ}_{1st}$ with a redistribution of charge that leads to an electron-rich surface.

In the case of the oxidized FeO_2-type surface terminations, the charges on the first layer oxygen ions are only slightly positive relative to bulk oxygen ions because, even under fully oxidized conditions, they are sufficiently coordinated by cations (their coordination number is 4). The O_{low} ions, however, are more undercoordinated than in the case of the LaO-type surface terminations (their coordination number is 1), and thus have relative Bader charges that are high relative to bulk oxygen ions. Stated differently, charge compensation to counter negative $\Delta\sigma^{\circ}_{1st}$ is achieved that results in a hole-rich surface.

The O_{low} relative charges for relaxed, oxidized FeO_2-type surface terminations are so much higher than in the case of their LaO-type surface termination counterparts because the surface region at the LaO surface termination is more electron rich than that at FeO_2 surface termination. Fig. 3(b) illustrated that the FeO_2 surface termination has fewer electrons than the LaO surface termination. Therefore, when additional undercoordinated O_{low} ions are added to the FeO_2-terminated surface during oxidation, there are fewer electrons available to them from the cations.

(B) Contributions of Sublayers to Charge Compensation: To investigate the contributions of subsurface layers (sublayers) to charge redistribution and compensation after surface relaxation, the Bader charges of all of the surface terminations are analyzed in terms of $\Delta\sigma_{1st}(=\sigma_{1st}-\sigma^{\circ}_{1st})$ and $-\Delta\sigma^{\circ}_{1st}(=\frac{1}{2}\sigma_B-\sigma^{\circ}_{1st})$ (see Fig. 9). Here, layer charges are mea-

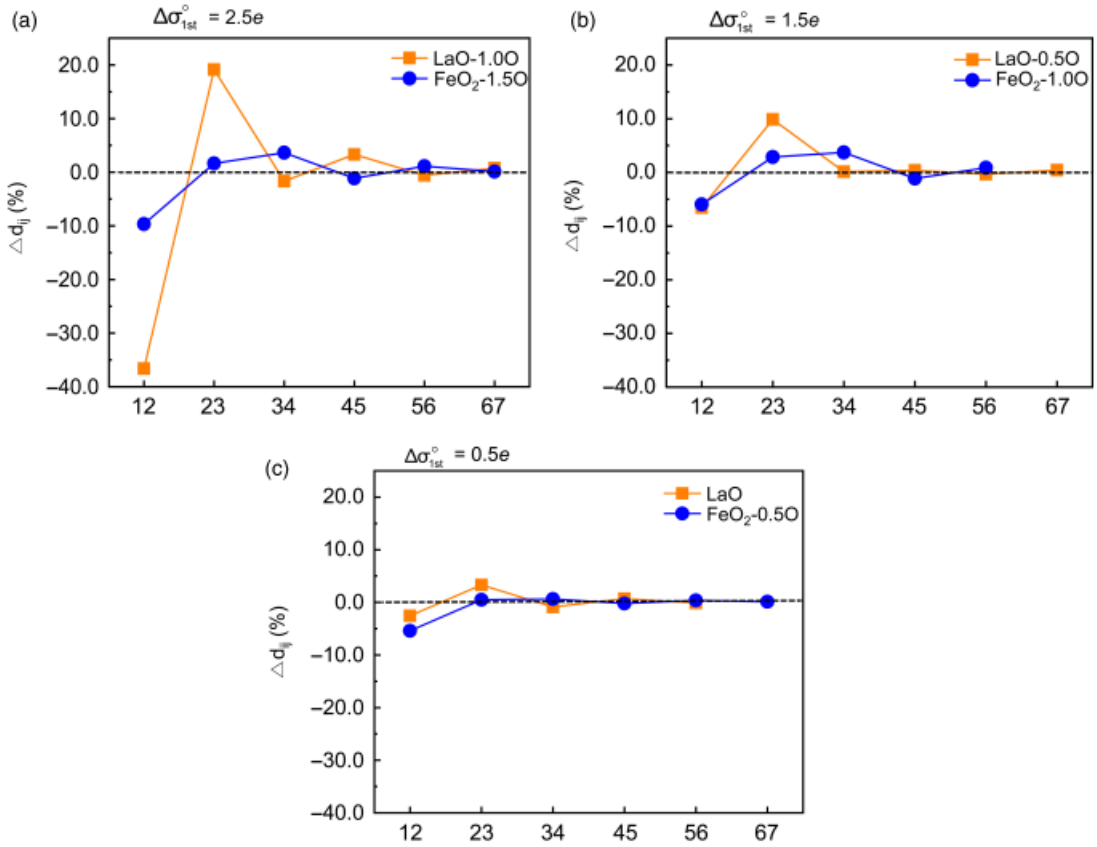

Fig. 10. Relative interlayer spacing of LaO-type and FeO_2-type surface terminations with respect to bulk interlayer spacing on (010) direction ($\Delta d_{ij}(\%)=\frac{d_{ij}-d^{bulkLFO}}{d^{bulkLFO}}\times 100$), where d_{ij} is the interlayer spacing between i-th and j-th layers and $d^{bulkLFO}$ is interlayer spacing of bulk LFO, 1.972 Å). Positive (negative) relaxation means expansion (contraction) of interlayer spacing. $\Delta\sigma^{\circ}_{1st}$ of each surface termination is determined by ideal ionic charges of La, Fe, and O in the bulk LFO. (a) Surface terminations with $\Delta\sigma^{\circ}_{1st}=2.5e$. (b) Surface terminations with $\Delta\sigma^{\circ}_{1st}=1.5e$. (c) Surface terminations with $\Delta\sigma^{\circ}_{1st}=0.5e$. X-axis shows layer numbers used for calculating Δd_{ij}. For example, y value for $x=12$ is Δd_{ij} for first and second layers.

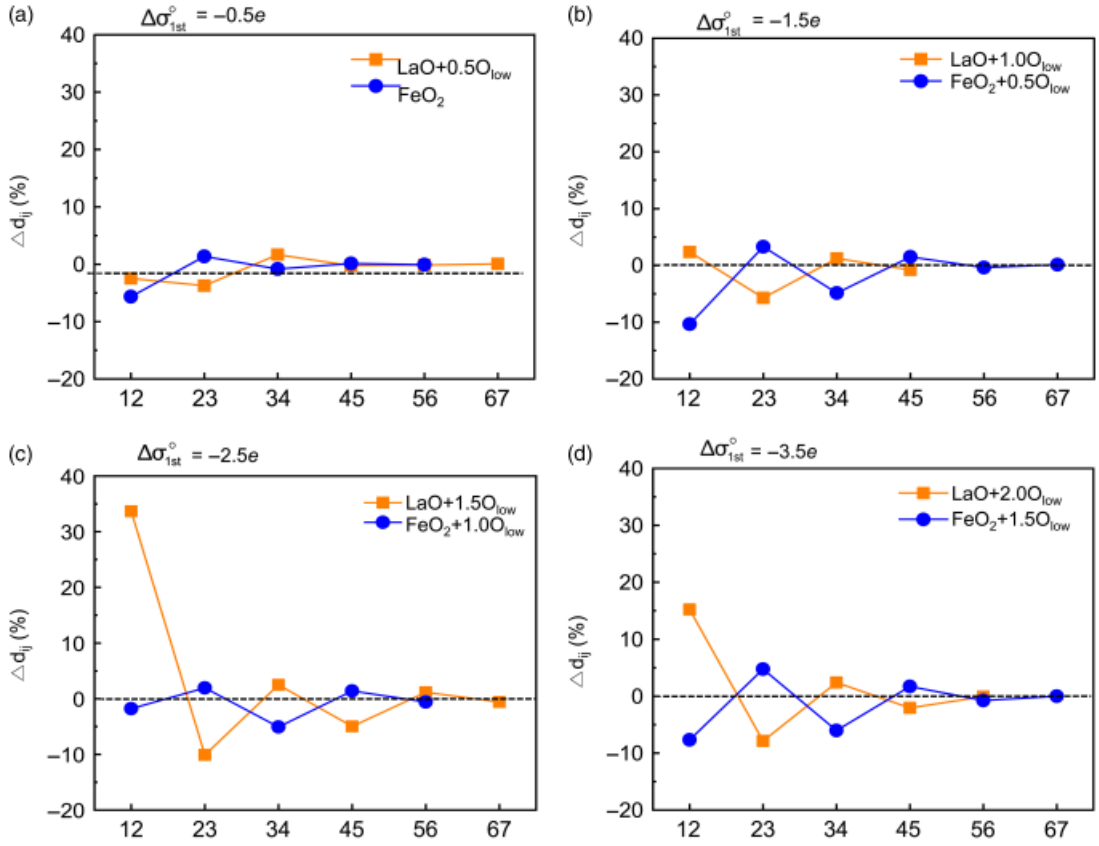

Fig. 11. Relative interlayer spacing of LaO-type and FeO_2-type surface terminations with respect to bulk interlayer spacing on (010) direction. Same setting from Fig. 10 is applied. (a) Surface terminations with $\Delta\sigma^{\circ}_{1st} = -0.5e$. (b) Surface terminations with $\Delta\sigma^{\circ}_{1st} = -1.5e$. (c) Surface terminations with $\Delta\sigma^{\circ}_{1st} = -2.5e$. (d) Surface terminations with $\Delta\sigma^{\circ}_{1st} = -3.5e$.

sured based on Bader charges. As $-\Delta\sigma^{\circ}_{1st}$ is the charge required to achieve charge compensation, and $\Delta\sigma_{1st}$ is the change of the charge within the first layer after electronic relaxation, we can define $\tau_{1st} = \frac{\Delta\sigma_{1st}}{-\Delta\sigma^{\circ}_{1st}} \times 100\,(\%)$ as a measure of the contribution of the first layer to the surface electronic redistribution. $\Delta\sigma^{\circ}_{1st,ideal}$ is calculated based on the ideal ionic charges of La, Fe, and O in bulk LFO, while $\Delta\sigma^{\circ}_{1st}$ is based on the Bader charges of these elements in the bulk.

Figure 9 indicates that reduced and stoichiometric LaO-type surface terminations have τ_{1st} that is less than 40%, while the reduced FeO_2-type surface terminations have τ_{1st} that range from 50% to 70% over the same range of $\Delta\sigma^{\circ}_{1st}$ values. This indicates that the contribution of sublayers to the charge compensation at the surface is more important for LaO-type than FeO_2-type surface terminations. For oxidized surfaces, the τ_{1st} of LaO-type surface terminations is consistently less than or equal to those of FeO_2-type surface terminations with the same $\Delta\sigma^{\circ}_{1st}$.

This contribution of electrons from the sublayers to the LaO-terminated surfaces lessens the extent to which the relative Bader charges of the O_{low} ions are positive relative to bulk oxygen ions. However, based on Fig. 3(b) the contribution of the sublayers to charge compensation of the FeO_2 surface termination with O_{low} atoms should be larger in magnitude than that of the LaO surface termination with O_{low} atoms. The reason is because the surface region of the stoichiometric FeO_2 surface termination is electron poor relative to the bulk region after charge redistribution.

In summary, the contribution of sublayers to charge compensation depends on surface stoichiometry. The contribution of sublayers to charge compensation is larger in reduced LaO-type surface terminations than in reduced FeO_2-type surface terminations (with positive $\Delta\sigma^{\circ}_{1st}$). For oxidized surfaces (with negative $\Delta\sigma^{\circ}_{1st}$), the contribution of sublayers to charge compensation in LaO-type surface terminations is greater than, or equal to, that in FeO_2-type surface terminations.

(C) Contribution of Atomic Relaxation to Charge Compensation: Atomic relaxation is described by the relative change in the interlayer spacing, $\Delta d_{ij}(\%) = \frac{d_{ij} - d^{bulkLFO}}{d^{bulkLFO}} \times 100$. Here, d_{ij} is the distance between the I-th and j-th layers along [010] direction; $d^{bulkLFO} = 1.972$ Å is the interlayer spacing along the [010] in bulk LFO. Figures 10 and 11 show how the layers of the surface slabs contribute to charge compensation. $\Delta\sigma^{\circ}_{1st}$ of each surface in the Figs. 10 and 11 is calculated based on the ideal ionic charges of La, Fe, and O in the bulk LFO. As illustrated in Fig. 10, the Δd_{ij} of LaO-type surface terminations are larger than those of the FeO_2-type surface terminations. Considering that the contribution of the sublayers to the charge compensation of reduced LaO-type surface terminations is larger than that of reduced FeO_2-type surface terminations, it can be deduced that the contributions of the sublayers to charge compensation is facilitated by atomic relaxation. For oxidized surface terminations, the interpretation of the contribution of atomic relaxation to surface charge compensation is not straightforward (see Fig. 11). For surface terminations with $\Delta\sigma^{\circ}_{1st} = -0.5e$ and $-2.5e$, the Δd_{ij} of LaO-type surface terminations are larger than those of FeO_2-type surface terminations with the same $\Delta\sigma^{\circ}_{1st}$. For surface terminations with $\Delta\sigma^{\circ}_{1st} = -1.5e$ and $-3.5e$, Δd_{ij} of LaO-type surface terminations are similar to those of FeO_2-type surface terminations. Consequently, atomic relaxation is generally larger for LaO-type surface terminations than for FeO_2-type surface terminations.

The strong atomic relaxation of LaO surface termination can be understood by a consideration of atomic packing and bond breaking at the surface. Based on Shannon radii, the LaO layer has a lower packing ratio (= 0.66) than the FeO_2 layer (= 0.84). Also, the stoichiometric LaO-terminated surface loses three bonds relative to the bulk when the surface is created (coordination number of La is reduced from 8 to 5), compared with the FeO_2-terminated surface, which loses one bond relative to the bulk (coordination number of Fe is reduced from 6 to 5). There-

fore, we would expect the LaO-terminated surface to relax more, which is what the calculations yield.

Nevertheless, the contribution of atomic relaxation is not always large for the LaO-type surface terminations. For instance, surfaces with $\Delta\sigma^{\circ}_{1st} = -1.5e$ and $-3.5e$ ($x = 1.0$ and 2.0), the Δd_{ij} of LaO-type and FeO_2-type surface terminations are similar. Figures 11(b) and (d) indicate that some surfaces with a higher number of O_{low} ions have less surface relaxation, which suggests that the O_{low} configurations may be influencing the relaxation process. However, additional study is required to fully determine this relationship.

IV. Conclusions

In conclusion, by changing the oxygen stoichiometry of the LFO (010) surface, we have dissected the stabilization of LFO (010) surfaces in terms of three factors: charge redistribution at the surface, the contribution of sublayers to charge compensation, and the contribution of atomic relaxation to charge compensation. All these factors are interrelated, but the results indicate that in the case of LaO-type surfaces, atomic relaxation is the most important factor because it facilitates charge redistribution of LaO-type surfaces. In the case of FeO_2-type surfaces, the ability of the Fe ion to modulate its valence makes charge redistribution at the surface more important.

The mechanisms identified allow two important predictions for the surface composition of the LFO (010) surface. First, the charge of La can change less easily than the charge of Fe and oxygen reduction should occur more readily on the FeO_2 surface termination than on the LaO surface termination. This may be one of the reasons that in ABO_3 perovskite cathode materials of SOFC, B site cations are catalytically more active than A site cations for oxygen reduction reactions.[44] This prediction provides us two possible strategies to promote oxygen reduction on the LFO (010) surfaces. One is to increase the stability of the FeO_2-type surfaces over the LaO-type terminations so that the FeO_2-type terminations are dominant during SOFC operating conditions, while the second is to improve the catalytic activity of the LaO surface by increasing the concentration of oxygen vacancies at the surface.

Even though this work focuses on pristine LFO surfaces, actual SOFC cathode materials are conductors due to the presence of dopants such as Sr and Co, which are likely to influence the electronic structure. To truly understand their contribution to the surface electronic redistribution, it requires analysis of the electronic structure of the doped surface. However, the analysis presented here allows us to make some qualitative predictions of the effect of these dopants on the LFO (010) surface. Assuming charge states for Sr and Co of 2+, the substitution of these dopants for cations will provide extra electrons to the material (Sr'_{La} and Co'_{Fe}). As a result, the $\Delta\sigma^{\circ}_{1st}$ values would be expected to become more negative than those of pristine LFO. Consequently, for surfaces with positive $\Delta\sigma^{\circ}_{1st}$, such as reduced terminations, fewer electrons would be required to achieve charge compensation in comparison with pure material. Therefore, it is likely that reduction is promoted by the presence of the dopants. Additionally, more holes would be needed for charge compensation at surfaces with negative $\Delta\sigma^{\circ}_{1st}$, such as oxidized surfaces, which would weaken electron transfer to the O_{low} atoms. This would serve to destabilize oxidized surfaces of doped LFO.

Acknowledgments

We acknowledge the University of Florida High-Performance Computing Center http://hpc.ufl.edu and EMSL, a national scientific user facility sponsored by the Department of Energy's Office (DOE) of Biological and Environmental Research and located at Pacific Northwest National Laboratory for providing computational resources for performing some of the calculations reported in this paper. C. L. thanks to Dr. Dongjo Oh (Hyundai Motors), Dr. Alex Tchernatinsky (UF), Prof. Dane Morgan, and Dr. Yueh-Lin Lee (University of Wisconsin-Madison) for fruitful discussions.

References

[1]S. B. Adler, "Factors Governing Oxygen Reduction in Solid Oxide Fuel Cell Cathodes," *Chem. Rev.*, **104** [10] 4791–844 (2004).
[2]R. Merkle and J. Maier, "Oxygen incorporation into Fe-Doped $SrTiO_3$: Mechanistic Interpretation of the Surface Reaction," *Phys. Chem. Chem. Phys.*, **4** [17] 4140–8 (2002).
[3]G. Kresse and J. Furthmüller, "Efficient Iterative Schemes for Ab Initio Total-Energy Calculations using a Plane-Wave Basis Set," *Phys. Rev. B*, **54** [16] 11169–86 (1996).
[4]G. Kresse and D. Joubert, "From Ultrasoft Pseudopotentials to the Projector Augmented-Wave Method," *Phys. Rev. B*, **59** [3] 1758–75 (1999).
[5]J. P. Perdew, K. Burke, and M. Ernzerhof, "Generalized Gradient Approximation Made Simple," *Phys. Rev. Lett.*, **77** [18] 3865–8 (1996).
[6]H. J. Monkhorst and J. D. Pack, "Special Points for Brillouin-Zone Integrations," *Phys. Rev. B*, **13** [12] 5188–92 (1976).
[7]V. I. Anisimov, F. Aryasetiawan, and A. I. Lichtenstein, "First-Principles Calculations of the Electronic Structure and Spectra of Strongly Correlated Systems: the LDA+ U Method," *J. Phys.: Condens. Matter*, **9** [4] 767–808 (1997).
[8]D. D. Cuong, B. Lee, K. M. Choi, H.-S. Ahn, S. Han, and J. Lee, "Oxygen Vacancy Clustering and Electron Localization in Oxygen-Deficient $SrTiO_3$: LDA+U Study," *Phys. Rev. Lett.*, **98** [11] 115503 (2007).
[9]L. Wang, T. Maxisch, and G. Ceder, "Oxidation Energies of Transition Metal Oxides within the GGA+U Framework," *Phys. Rev. B*, **73** [19] 195107 (2006).
[10]A. Barbier, A. Stierle, N. Kasper, M. J. Guittet, and J. Jupille, "Surface Termination of Hematite at Environmental Oxygen Pressures: Experimental Surface Phase Diagram," *Phys. Rev. B*, **75** [23] 233406 (2007).
[11]N. Sakai, K. Yamaji, T. Horita, Y. P. Xiong, H. Kishimoto, M. E. Brito, and H. Yokokawa, "Erratum to "Effect of Water on Electrochemical Oxygen Reduction at the Interface Between Fluorite-Type Oxide-Ion Conductors and Various Types of Electrodes"," *Solid State Ionics*, **176** [29–30] 2327–33 (2005).
[12]K. Reuter and M. Scheffler, "Composition, Structure, and Stability of RuO_2(110) as a Function of Oxygen Pressure," *Phys. Rev. B*, **65** [3] 035406 (2001).
[13]X. G. Wang, W. Weiss, S. K. Shaikhutdinov, M. Ritter, M. Petersen, F. Wagner, R. Schlöl, and M. Scheffler, "The Hematite (a-Fe_2O_3) (0001) Surface: Evidence for Domains of Distinct Chemistry," *Phys. Rev. Lett.*, **81** [5] 1038 (1998).
[14]X.-G. Wang, A. Chaka, and M. Scheffler, "Effect of the Environment on Alpha-Al_2O_3 (0001) Surface Structures," *Phys. Rev. Lett.*, **84** [16] 3650 (2000).
[15]E. A. Kotomin, Y. A. Mastrikov, E. Heifets, and J. Maier, "Adsorption of Atomic and Molecular Oxygen on the $LaMnO_3$(001) Surface: Ab initio Supercell Calculations and Thermodynamics," *Phys. Chem. Chem. Phys.*, **10** [31] 4644–9 (2008).
[16]Y. A. Mastrikov, E. Heifets, E. A. Kotomin, and J. Maier, "Atomic, Electronic and Thermodynamic Properties of Cubic and Orthorhombic $LaMnO_3$ Surfaces," *Surf. Sci.*, **603** [2] 326–35 (2009).
[17]X. Liu, J. Hu, B. Cheng, H. Qin, M. Zhao, and C. Yang, "First-Principles Study of O_2 Adsorption on the $LaFeO_3$ (010) Surface," *Sens. Actuators B*, **139** [2] 520–6 (2009).
[18]Y.-L. Lee, J. Kleis, J. Rossmeisl, and D. Morgan, "Ab Initio Energetics of $LaBO_3$ (001) (B = Mn, Fe, Co, and Ni) for Solid Oxide Fuel Cell Cathodes," *Phys. Rev. B*, **80** [22] 224101 (2009).
[19]R. H. Mitchell, *Perovskites Modern and Ancient*. Almaz Press, Thunder Bay, ON, 2002.
[20]J. L. Wohlwend, R. K. Behera, I. Jang, S. R. Phillpot, and S. B. Sinnott, "Morphology and Growth Modes of Metal-Oxides Deposited on $SrTiO_3$," *Surf. Sci.*, **603** [6] 873–80 (2009).
[21]H. Kawanowa, H. Ozawa, M. Ohtsuki, Y. Gotoh, and R. Souda, "Structure Analysis of $LaAlO_3$(0 0 1) Surfaces by Low Energy Neutral Scattering Spectroscopy," *Surf. Sci.*, **506** [1–2] 87–92 (2002).
[22]R. I. Eglitis and V. David, "Ab initio Calculations of $BaTiO_3$ and $PbTiO_3$ (001) and (011) Surface Structures," *Phys. Rev. B*, **76** [15] 155439 (2007).
[23]G. Borstel, R. I. Eglitis, E. A. Kotomin, and E. Heifets, "Modelling of Defects and Surfaces in Perovskite Ferroelectrics," *Phys. Status Solidi (B)*, **236** [2] 253–64 (2003).
[24]C. H. Lanier, A.van de Walle, N. Erdman, E. Landree, O. Warschkow, A. Kazimirov, K. R. Poeppelmeier, J. Zegenhagen, M. Asta, and L. D. Marks, "Atomic-Scale Structure of the $SrTiO_3$(001)-c(6×2) Reconstruction: Experiments and First-Principles Calculations," *Phys. Rev. B*, **76** [4] 045421–9 (2007).
[25]C. H. Lanier, J. M. Rondinelli, B. Deng, R. Kilaas, K. R. Poeppelmeier, and L. D. Marks, "Surface Reconstruction with a Fractional Hole: ($\sqrt{(5)} \times \sqrt{(5)}$)R26.6° $LaAlO_3$ (001)," *Phys. Rev. Lett.*, **98** [8] 086102 (2007).
[26]J.-L. Tang, J. Zhu, W.-F. Qin, J. Xiong, Y. Zhang, and Y.-R. Li, "Atomic Relaxation and Electronic Redistribution of $LaAlO_3$(001) Surfaces," *Phys. Lett. A*, **365** [1–2] 149–55 (2007).
[27]J. He, R. K. Behera, M. W. Finnis, X. Li, E. C. Dickey, S. R. Phillpot, and S. B. Sinnott, "Prediction of High-Temperature Point Defect Formation in TiO_2 from Combined ab initio and Thermodynamic Calculations," *Acta Mater.*, **55** [13] 4325–37 (2007).
[28]K. Johnston, M. R. Castell, A. T. Paxton, and M. W. Finnis, "$SrTiO_3$ (001) (2×1) Reconstructions: First-Principles Calculations of Surface Energy and Atomic Structure Compared with Scanning Tunneling Microscopy Images," *Phys. Rev. B*, **70** [8] 085415 (2004).
[29]P. W. Tasker, "The Stability of Ionic Crystal Surfaces," *J. Phys. C*, **12** [22] 4977–84 (1979).
[30]C. Noguera, *Physics and Chemistry at Oxide Surfaces*. Cambridge University Press, Cambridge, 1995.
[31]C. Noguera, "Polar Oxide Surfaces," *J. Phys.: Condens. Matter*, **12** [31] R367 (2000).

[32]H. Falcon, A. E. Goeta, G. Punte, and R. E. Carbonio, "Crystal Structure Refinement and Stability of $LaFe_xNi_{1-x}O_3$ Solid Solutions," *J. Solid State Chem.*, **133** [2] 379–85 (1997).

[33]C. Filippi, D. J. Singh, and C. J. Umrigar, "All-Electron Local-Density and Generalized-Gradient Calculations of the Structural Properties of Semiconductors," *Phys. Rev. B*, **50** [20] 14947 (1994).

[34]R. Shannon, "Revised Effective Ionic Radii and Systematic Studies of Interatomic Distances in Halides and Chalcogenides," *Acta Crystallogr. Sect. A: Found. Crystallogr.*, **32** [5] 751–67 (1976).

[35]T. Arima, Y. Tokura, and J. B. Torrance, "Variation of Optical Gaps in Perovskite-Type 3D Transition-Metal Oxides," *Phys. Rev. B*, **48** [23] 17006 (1993).

[36]P. Ravindran, R. Vidya, H. Fjellv, and A. Kjekshus, "Electronic Structure and Excited-State Properties of Perovskite-Like Oxides," *J. Cryst. Growth*, **268** [3–4] 554–9 (2004).

[37]D. D. Sarma, N. Shanthi, S. R. Barman, N. Hamada, H. Sawada, and K. Terakura, "Band Theory for Ground-State Properties and Excitation Spectra of Perovskite $LaMO_3$ (M = Mn, Fe, Co, Ni)," *Phys. Rev. Lett.*, **75** [6] 1126 (1995).

[38]C. Zhong, X. Jiang, H. Yu, Q. Jiang, J. Fang, and Z. Li, "First-Principles Studies of the Magnetic Structure and Exchange Interactions in the Frustrated Multiferroic $YMnO_3$," *J. Magn. Magn. Mater.*, **321** [9] 1260–5 (2009).

[39]W. C. Koehler, E. O. Wollan, and M. K. Wilkinson, "Neutron Diffraction Study of the Magnetic Properties of Rare-Earth-Iron Perovskites," *Phys. Rev.*, **118** [1] 58 (1960).

[40]D. Treves, "Studies on Orthoferrites at the Weizmann Institute of Science," *J. Appl. Phys.*, **36** [3] 1033–9 (1965).

[41]A. Fossdal, M. Menon, I. Wærnhus, K. Wiik, M.-A. Einarsrud, and T. Grande, "Crystal Structure and Thermal Expansion of $La_{1x}Sr_xFeO_{3\delta}$ Materials," *J. Am. Ceram. Soc.*, **87** [10] 1952–8 (2004).

[42]J. W. Seo, E. E. Fullerton, F. Nolting, A. Scholl, J. Fompeyrine, and J.-P. Locquet, "Antiferromagnetic $LaFeO_3$ Thin Films and their Effect on Exchange Bias," *J. Phys.: Condens. Matter*, **20** [26] 264014 (2008).

[43]R. Bader, *Atoms in Molecules: A Quantum Theory*. Oxford University Press, New York, 1990.

[44]Y. Takeda, R. Kanno, M. Noda, Y. Tomida, and O. Yamamoto, "Cathodic Polarization Phenomena of Perovskite Oxide Electrodes with Stabilized Zirconia," *J. Electrochem. Soc.*, **134** [11] 2656–61 (1987). □